Nanoscale

Accepted Manuscript

This article can be cited before page numbers have been issued, to do this please use: E. Bergeron, S. Patskovsky, D. Rioux and M. Meunier, *Nanoscale*, 2016, DOI: 10.1039/C6NR01257D.

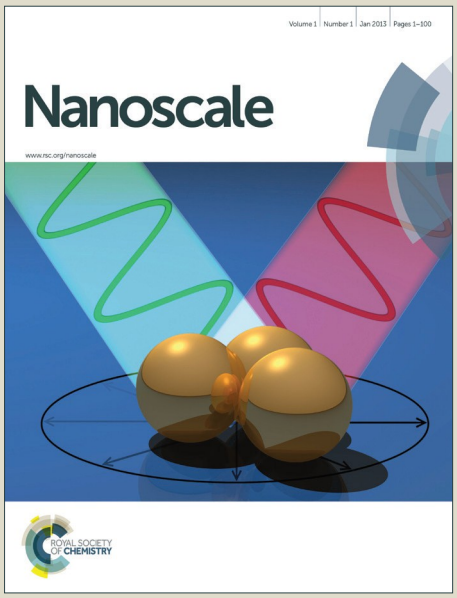

This is an *Accepted Manuscript*, which has been through the Royal Society of Chemistry peer review process and has been accepted for publication.

Accepted Manuscripts are published online shortly after acceptance, before technical editing, formatting and proof reading. Using this free service, authors can make their results available to the community, in citable form, before we publish the edited article. We will replace this *Accepted Manuscript* with the edited and formatted *Advance Article* as soon as it is available.

You can find more information about *Accepted Manuscripts* in the Information for Authors.

Please note that technical editing may introduce minor changes to the text and/or graphics, which may alter content. The journal's standard Terms & Conditions and the Ethical guidelines still apply. In no event shall the Royal Society of Chemistry be held responsible for any errors or omissions in this *Accepted Manuscript* or any consequences arising from the use of any information it contains.

ROYAL SOCIETY OF CHEMISTRY

www.rsc.org/nanoscale

View Article Online
DOI: 10.1039/C6NR01257D

Nanoscale

ARTICLE

3D multiplexed immunoplasmonics microscopy

Éric Bergeron,[a] Sergiy Patskovsky,[a] David Rioux[a] and Michel Meunier*[a]

Received 00th January 20xx,
Accepted 00th January 20xx

DOI: 10.1039/x0xx00000x

www.rsc.org/

Selective labelling, identification and spatial distribution of cell surface biomarkers can provide important clinical information, such as distinction between healthy and diseased cells, evolution of a disease and selection of the optimal patient-specific treatment. Immunofluorescence is the gold standard for efficient detection of biomarkers expressed by cells. However, antibodies (Abs) conjugated to fluorescent dyes remain limited by photobleaching, high sensitivity to the environment, low light intensity, and wide absorption and emission spectra. Immunoplasmonics is a novel microscopy method based on the visualization of Abs-functionalized plasmonic nanoparticles (fNPs) targeting cell surface biomarkers. Tunable fNPs should provide higher multiplexing capacity than immunofluorescence since NPs are photostable over time, strongly scatter light at their plasmon peak wavelengths and can be easily functionalized. In this article, we experimentally demonstrate accurate multiplexed detection based on immunoplasmonics approach. First, we achieve the selective labelling of three targeted cell surface biomarkers (cluster of differentiation 44 (CD44), epidermal growth factor receptor (EGFR) and voltage-gated K^+ channel subunit $K_V1.1$) on human cancer $CD44^+$ $EGFR^+$ $K_V1.1^+$ MDA-MB-231 cells and reference $CD44^-$ $EGFR^-$ $K_V1.1^+$ 661W cells. The labelling efficiency with three stable specific immunoplasmonics labels (functionalized silver nanospheres (CD44-AgNSs), gold (Au) NSs (EGFR-AuNSs) and Au nanorods ($K_V1.1$-AuNRs)) detected by reflected light microscopy (RLM) is similar to the one with immunofluorescence. Second, we introduce an improved method for 3D localization and spectral identification of fNPs based on fast z-scanning by RLM with three spectral filters corresponding to the plasmon peak wavelengths of the immunoplasmonics labels in the cellular environment (500 nm for 80 nm AgNSs, 580 nm for 100 nm AuNSs and 700 nm for 40 nm x 92 nm AuNRs). Third, the developed technology is simple and compatible with standard epi-fluorescence microscopes used in biological and clinical laboratories. Thus, 3D multiplexed immunoplasmonics microscopy is ready for clinical applications as a cost-efficient alternative to immunofluorescence.

1. Introduction

Selective labelling, identification and spatial distribution of cell surface biomarkers can provide important information for cell biology and clinical applications, such as distinction between healthy and diseased cells, early detection of a disease, evolution of a disease at different stages, selection of the optimal patient-specific treatment and monitoring of the therapeutic response.[1,2] The current gold standard for efficient detection of biomarkers expressed by cells is immunofluorescence, which is based on fluorescent dyes conjugated to antibodies (Abs). However, fluorescent dyes remain limited by photobleaching, high sensitivity to the environment, low light intensity, and wide absorption and emission spectra.[3–6] Since most primary Abs are developed in mice, rats and rabbits, and each secondary Abs should recognize only primary Abs developed in a specific species, the simultaneous multiplexing capacity of immunofluorescence remains limited. Since fluorescent dyes are mainly developed in the narrow range of the visible wavelengths (λ = 400–700 nm),[5,7] the upper limit of fluorescent dye-based multiplexing is about ~7 with statistical and graphical procedures and deconvolution.[5] With the advent of nanotechnology, simultaneous excitation of functionalized quantum dots (QDs) has emerged as a powerful substitute to fluorescent dyes for multiplexing applications.[6] QDs exhibit size-tunable fluorescence colour, high brightness, narrow emission and stability against photobleaching, but they suffer from blinking and potential toxicity with autofluorescent cells.[7]

Plasmonic nanoparticles (NPs) made of gold (Au) or silver (Ag) offer various interesting properties that can overcome some of the issues observed with fluorescence-based labels. NPs are well-suited for optical detection and treatment of diseased cells since they are photostable over time, strongly scatter light at their plasmon peak wavelengths and can be easily functionalized with Abs or aptamers.[2,3,5,8–11] AuNPs are biocompatible both *in vitro*[12] and *in vivo*,[13] and AgNPs can become biocompatible with proper functionalization.[14] AgNPs offer greater spectral contrast than AuNPs, but they are more difficult to synthesize with controllable homogeneous shape and size.[15] The scattering peak wavelengths of Ag and Au nanospheres (NSs) are around 400–500 and 520–570 nm,

[a] *Laser Processing and Plasmonics Laboratory, Department of Engineering Physics, Polytechnique Montréal, C.P. 6079, Succursale Centre-Ville, Montréal, QC, H3C 3A7, Canada. E-mail: michel.meunier@polymtl.ca*

Electronic Supplementary Information (ESI) available: Characterization of functionalized nanoparticles by UV-visible-NIR spectroscopy, standard darkfield microscopy and reflected light microscopy. Immunofluorescence of cells.
See DOI: 10.1039/x0xx00000x

View Article Online
DOI: 10.1039/C6NR01257D

respectively, and the ones from Au nanorods (AuNRs) can be extended from 600 to 2200 nm by tuning their aspect ratio (length/diameter).[9] The spectral tunability of NPs should thus provide high multiplexing capacity since up to 19 types of NPs can be used in the 400–2200 nm range with a 100 nm distance between their scattering peaks.

In order to propose plasmonic NP optical labels as an alternative to fluorescent dyes, it is crucial to consider how they can target established biomarkers with high affinity. Plasmonic NPs are commonly functionalized with poly(ethylene glycol) (PEG) and Abs[11,16,17] for successful targeting of cell surface biomarkers expressed by cancer cells, such as the epidermal growth factor receptor (EGFR)[18,19] and the cluster of differentiation 44 (CD44).[20–23] For example, human breast cancer MDA-MB-231 cells express EGFR[24] and CD44.[20,25] We previously targeted and imaged in 2D and 3D these cells with 100 nm AuNSs functionalized sequentially with orthopyridyl-disulfide (OPSS)-PEG(5 kDa)-Abs anti-CD44 and HS-PEG (2 or 5 kDa).[22,23] Another important factor to consider for efficient selective detection of targeted biomarkers is the stability of Abs-functionalized plasmonic NPs (fNPs) since serum proteins in the cellular environment can adsorb non-specifically on NPs.[26] We recently demonstrated that CD44-AuNSs were more stable with 5 kDa HS-PEG than with 2 kDa HS-PEG under physiological conditions of pH and salinity.[20] The multiplexing capacity can be further increased with fNPs functionalized with surface-enhanced Raman scattering (SERS) reporter molecules.[27] The characteristic narrow Raman signatures allow the identification and quantification of various biomarkers, but their acquisition by Raman spectroscopy requires more complex equipment than epi-fluorescence microscope.[28]

In regards to the optical detection and localization of the highly diffusive NPs in the cellular environment, the most efficient methods are laser scanning confocal microscopy[15,29] and darkfield microscopy.[19,20] The discrimination of plasmonic labels is based on the analysis of the scattered light since their spectral profiles depend on the NP's composition, size, shape, clustering state and surrounding refractive index (RI) environment.[30] Several commercial hyperspectral research systems (CytoViva, Auburn, AL, U.S.A.; PARISS, Asheville, NC, U.S.A.; Photon Etc., Montreal, QC, Canada) provide highly accurate spectral characterization of NPs to ensure reliable identification of multiple NPs in various environments.

The reliability of standard fluorescence spectroscopy is based on highly efficient spectral separation between the fluorescence emission and the excitation light. In order to provide an improved performance compared to immunofluorescence, immunoplasmonics microscopy based on plasmonic NP backscattering must detect and spectrally identify each single NP.[31] Since cell biologists and clinical pathologists investigate samples with thickness up to 20 µm, the 3D distribution of NPs needs to be visualized for sample characterization. Confocal or darkfield microscopy with an additional z-scan can perform such 3D NPs imaging. However, the time, cost and sample preparation involved in this analysis limit the transfer of these technologies into routine tests. The ideal 3D NPs imaging system should be simple, low cost and complementary to the existing epi-fluorescence microscopes to allow different tests on the same platform.

We propose a solution based on spectrally modulated reflected light microscopy (RLM)[22,23] with a high numerical aperture (NA) objective and z-scanning mode that can provide fast localization and spectral identification of each fNP (Fig. 1). RLM is simple and compatible with epi-fluorescence microscopy for easy integration into existing set-ups. Since the light scattered from the cells is reduced in this optical configuration in comparison to standard darkfield imaging, RLM of cellular samples contributes to enhance the contrast of fNPs over the cells. The proposed RLM is equipped with a high NA objective which ensures fast and precise 3D mapping of the fNPs in combination with rapid algorithms for high-resolution 2D[8] and 3D[32] localization of each single fNP.

In this work, we show a 3D multiplexed immunoplasmonics approach by using CD44-AgNSs, EGFR-AuNSs and K_V1.1-AuNRs as optical labels which provides an optimal spectral separation and can be tuned to cover the visible range of standard optical detectors. As an example, we show fast localization and identification of three different stable fNPs targeting cell surface biomarkers as an alternative to immunofluorescence.

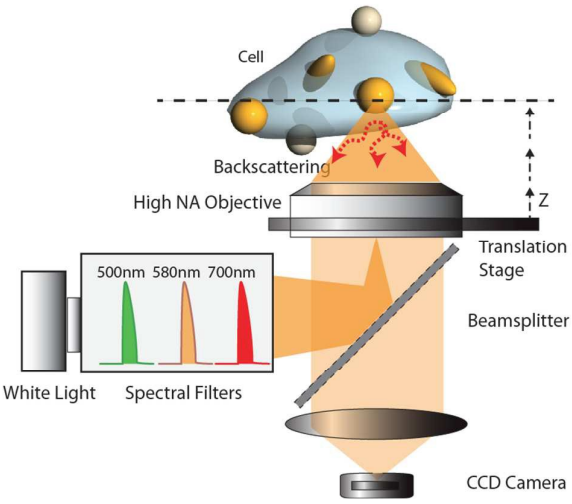

Fig. 1 RLM set-up for 3D wide-field imaging of fNPs in cellular environment. Spectral filters are centered around the average plasmon peak wavelength of each type of fNP: 500 nm for AgNS, 580 nm for AuNS and 700 nm for AuNR.

2. Results and discussion

2.1 Choice of NP immunoplasmonics labels

Simplicity of the application and the performance of multiplexed immunoplasmonics microscopy depend on the optical detection method and the choice of fNPs. Here, the three labels should show similar scattering efficiency and the spectral position of their resonance peaks should be observed in the detection range of a standard monochromatic CCD camera (400–800 nm). To target cell surface biomarkers, stable fNPs have to be large (>75 nm) in order to offer high

View Article Online
DOI: 10.1039/C6NR01257D

light scattering, low cell internalization and single localization without aggregation in the cellular environment. Such fNPs strongly scatter light at their plasmon peak wavelengths, which facilitates optical detection, but their wide resonance plasmon peaks decrease the spectral discrimination ability in multiplexing applications. We have theoretically calculated (with Mie theory[33], COMSOL software (Burlington, MA, U.S.A.) and dielectric functions for Au[34] and Ag[35]) and experimentally confirmed that 80 nm AgNS, 100 nm AuNS and 40 nm x 92 nm AuNR offer optimal compromise between all these criteria (Fig. 2A and Table S1).

2.2 Preparation of stable functionalized NPs and selective cell targeting

A very important requirement for fNPs as immunoplasmonics labels is their stability and resistance to aggregation in a complex cellular environment. Citrate-capped plasmonic NPs aggregate rapidly upon treatment with 1% (w/v) aqueous NaCl, a solution that is approximately isotonic with normal human plasma.[36] Aggregation can be detected by monitoring the intensity of the NPs' plasmon band.

Fig. 2 (A) Theoretical backscattering spectra for the selected NPs in water (blue line: AgNS, orange line: AuNS, red line: 40 nm x 92 nm AuNR). (B-D) Representative experimental UV-visible-NIR spectra of bare NPs and fNPs with OPSS-PEG-Ab and HS-PEG: CD44-AgNSs (B, n = 7), EGFR-AuNSs (C, n = 6) and K_V1.1-AuNRs (D, 40 nm x 92 nm, n = 1; 53 nm x 107 nm, n = 4). Samples before purification or after centrifugation and resuspension in phenol red-free DMEM were incubated for 30 min in water or 1% NaCl.

After 30 min, the band intensity of AgNSs, AuNSs and AuNRs decreased by 82%, 70% and 71% in saline environment compared to NPs dispersed in water, respectively. Stable PEGylated NPs in 1% NaCl were obtained with 40 µM HS-PEG (5 kDa) with no loss of intensity (Fig. S1).

We then confirmed that the previous reported procedure[20] to functionalize AuNSs with Abs anti-CD44 can be extended to various plasmonic NPs and Abs. Abs linked to OPSS-PEG(5 kDa)-NHS (OPSS-PEG-Ab) were incorporated at a level of 0.45% (v/v) to the citrate-capped NPs during 1 h, then incubated with 40 µM HS-PEG (5 kDa). The NPs functionalized with different Abs were stable in saline environment similar to physiological conditions (Fig. 2 and S2). The efficient coating was further confirmed by a red-shift of the fNPs' plasmon peaks with a moderate loss of intensity in comparison to citrate-capped NPs' plasmon peak in water (Fig. 2 and S2). Batches of fNPs were subjected to centrifugation immediately after synthesis in order to isolate the fNPs and resuspend them in phenol red-free Dulbecco's Modified Eagle's Medium (DMEM), the cell culture medium used in the *in vitro* experiments. These purified fNPs remained stable in saline environment (Fig. 2 and S2).

The selectivity and stability of purified fNPs (CD44-AgNSs, EGFR-AuNSs and K_V1.1-AuNRs) were verified with $CD44^+$ $EGFR^+$ $K_V1.1^+$ MDA-MB-231 and $CD44^-$ $EGFR^-$ $K_V1.1^+$ 661W cells cultured in DMEM containing 10% (v/v) fetal bovine serum (FBS). After 3 h incubation, living cells were washed three times with phosphate-buffered saline (PBS) to remove unbound fNPs.[20] Standard darkfield microscopy[20] confirmed

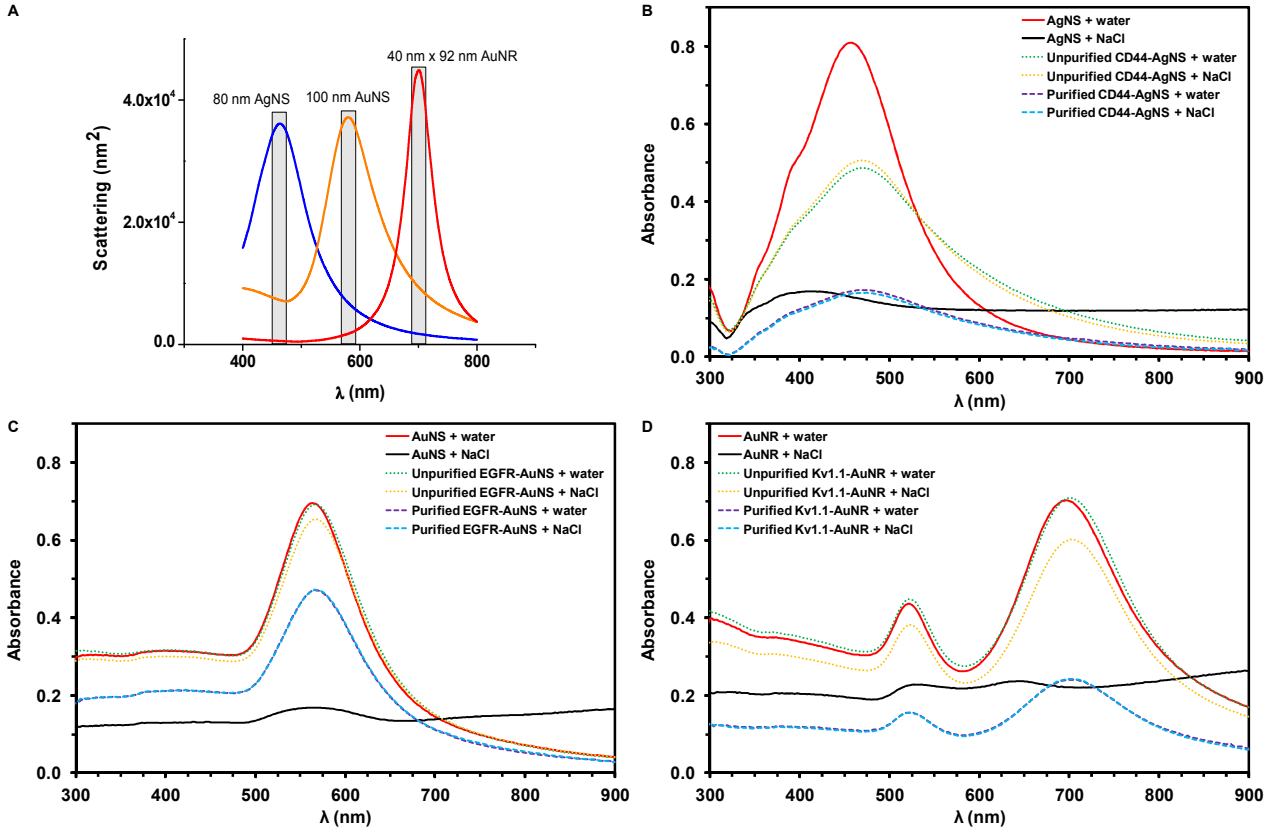

View Article Online
DOI: 10.1039/C6NR01257D

selective targeting of CD44-overexpressing MDA-MB-231 cells with CD44-AgNPs, CD44-AuNPs and CD44-AuNRs (Fig. S3). Since EGFR-AuNSs and $K_V1.1$-AuNRs were weakly detected on $EGFR^+$ $K_V1.1^+$ MDA-MB-231 cells by standard darkfield microscopy, a more robust imaging technique based on RLM was used.

2.3 3D wide-field fNP imaging in cellular environment

Our RLM optical set-up for wide-field 3D imaging was used to estimate the total number of fNPs selectively labelling the targeted cell surface biomarkers. First, we recorded the sequence of optical section images taken at different z positions with 100 nm step in a narrow spectral range (580 nm spectral filter for EGFR-AuNS). The resulting typical experimental 3D and 2D intensity profiles of cells targeted with fNPs obtained at different focal planes are presented in Fig. 3. A 1.3 NA objective in backreflection provides a high contrast of the fNPs over the cells and allows precise 3D fNPs localization (Fig. 3A,B).[23] The method's reliability for fNPs quantification is improved by applying numerical 3D deconvolution (ImageJ) using experimental point spread function (PSF) (Fig. S4). The non-uniform background created by cells' light scattering is removed from the images (Fig. 3C,D), thus enhancing the fNPs contrast over cells. 3D image of EGFR-AuNSs on $CD44^+$ $EGFR^+$ $K_V1.1^+$ MDA-MB-231 cells obtained with 100 nm step z-scan by RLM set-up with consecutive image deconvolution is shown in Fig. S5. The real-time animation for 3D microscopy scan of EGFR-AuNSs on the cells can be found in Video S1, and the corresponding 2D image obtained by z-stacks' integration from this video is presented in Fig. S6. Here, we applied ImageJ 3D Viewer plug-in for the final image data treatment and visualization.

Fig. 3 Example of optical sectioning by using z-scan in the proposed RLM set-up. 3D (A,C) and 2D (B,D) intensity profiles of EGFR-AuNSs on $CD44^+$ $EGFR^+$ $K_V1.1^+$ MDA-MB-231 cells obtained at three different planes separated by 4 µm (Objective 100×). (C,D) Deconvolution of the images using experimental PSFs.

A consecutive application of local maximum filtering and 3D Object Counter (ImageJ) was used to obtain the total number and 3D position of fNPs proportional to the relative concentration of the targeted biomarkers. An image of a cell taken by annular oblique illumination combined with calculated 3D fNPs position is shown in Fig S5C. Spatial position and distribution of fNPs can be useful to estimate the local concentration and clustering state of targeted biomarkers.

2.4 Spectroscopy of single fNPs in cellular environment

Experimental verification of the spectral characteristics and potential discrimination contrast provided by fNPs was performed by using RLM optical set-up for fNPs microspectroscopy. We evaluated backscattering spectra of single CD44-AgNSs, EGFR-AuNSs and $K_V1.1$-AuNRs selectively attached to targeted biomarkers expressed by MDA-MB-231 cells. Spectra of NPs in water were also measured for comparison. Mie theory was applied to obtain theoretical scattering spectra of NPs in mediums with different RI, and AuNR spectrum was evaluated by COMSOL software (Fig. 4). The experimental plasmon peaks of CD44-AgNSs in the cellular environment were located around 472–487 nm and were red-shifted by ~16 nm relative to the plasmon peak wavelength of bare AgNSs in water at 464 nm (close to the predictions by Mie theory) (Fig. 4A). The theoretical plasmon peak position of AuNSs in water was about 580 nm. After functionalization and attachment to the cells, the scattering peaks of EGFR-AuNSs were red-shifted to 587–597 nm (Fig. 4B). The theoretical plasmon peak position of bare AuNRs was 700 nm and showed a larger experimental distribution from 660 to 700 nm. The $K_V1.1$-AuNRs presented red-shifts to 713–734 nm in the cellular environment (Fig. 4C). Our calculations show that for each type of NPs, the observed experimental plasmon peak red-shifts can be explained by a change of the local RI (to 1.37 – 1.43) due to the NP functionalization with OPSS-PEG-Ab (RI = 1.49) and thiolated PEG chains (RI = 1.46)[20], and the interactions with the complex cellular environment containing proteins, sugars and different biomolecules.

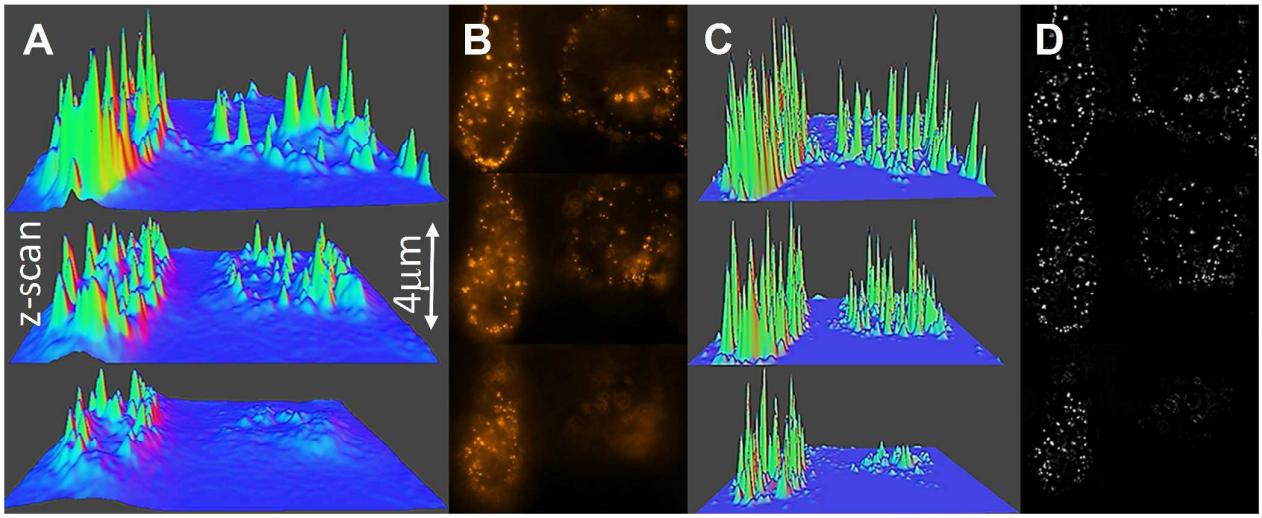

View Article Online
DOI: 10.1039/C6NR01257D

Microspectroscopy of single fNPs showed that EGFR-AuNSs are stable, with high optical contrast and low level of aggregation. CD44-AgNSs also provide high optical contrast, but 10–15% of them were aggregated (Fig. S7A). Further optimization of their functionalization and stabilization can contribute to decrease their size heterogeneity in biological environment. $K_V1.1$-AuNRs are stable, with low level of aggregation. Since AuNRs can attach to the targeted biomarkers in random orientation, the scattering intensity and experimental optical contrast can vary between these optical labels, especially with polarized light detection (Fig. S7B). This spatial effect is low in RLM since the illumination uses unpolarised light and the high NA objective provides a wide range of angles for illumination and detection.

Fig. 4. Normalized scattering spectra of CD44-AgNSs (A, n = 5), EGFR-AuNSs (B, n = 11) and $K_V1.1$-AuNRs (40 nm x 92 nm, C, n = 9) measured by RLM. Theoretical (dashed line) and experimental spectra (coloured lines) of fNPs. Black symbols show experimental intensities obtained with three spectral filters: 500, 580 and 700 nm. (D) Normalized experimental scattering spectra from panels A, B and C at 500, 580 and 700 nm for the construction of the look-up table for fNP discrimination.

2.5 3D multiplexed reflected light microscopy

In this article, we propose multiplexed immunoplasmonics microscopy based on the precise 3D localization of fNPs by RLM and simplified spectral discrimination of three plasmonic labels using 3 points spectral analysis. To prove such methodology, we present data obtained by 3D cells-fNPs scanning with three different spectral filters. It allows the detection of three different optical labels targeting cell surface biomarkers on a cellular sample. Experimentally, $CD44^+$ $EGFR^+$ $K_V1.1^+$ MDA-MB-231 and $CD44^-$ $EGFR^-$ $K_V1.1^+$ 661W cells were incubated during 3 h with CD44-AgNSs, EGFR-AuNSs and $K_V1.1$-AuNRs, washed, fixed and observed with 3D RLM and the spectral filters at 500, 580 and 700 nm.

First, we needed to establish a look-up table to quickly identify the type of each detected optical label (CD44-AgNS, EGFR-AuNS or $K_V1.1$-AuNR) based on the light scattering intensities measured with the spectral filters. Using the method described in section 2.3, we calculated the total number of fNPs and merged the resulting three tables with 3D coordinates (x,y,z) of each single fNP. All localizations of fNPs in duplicate were removed and final data were completed with the corresponding intensity data measured with the spectral filters. The intensities obtained with the three optical filters were compared to confirm the type of each single fNP. In Fig. 4A-C, colour symbols (squares, triangles and circles) show the

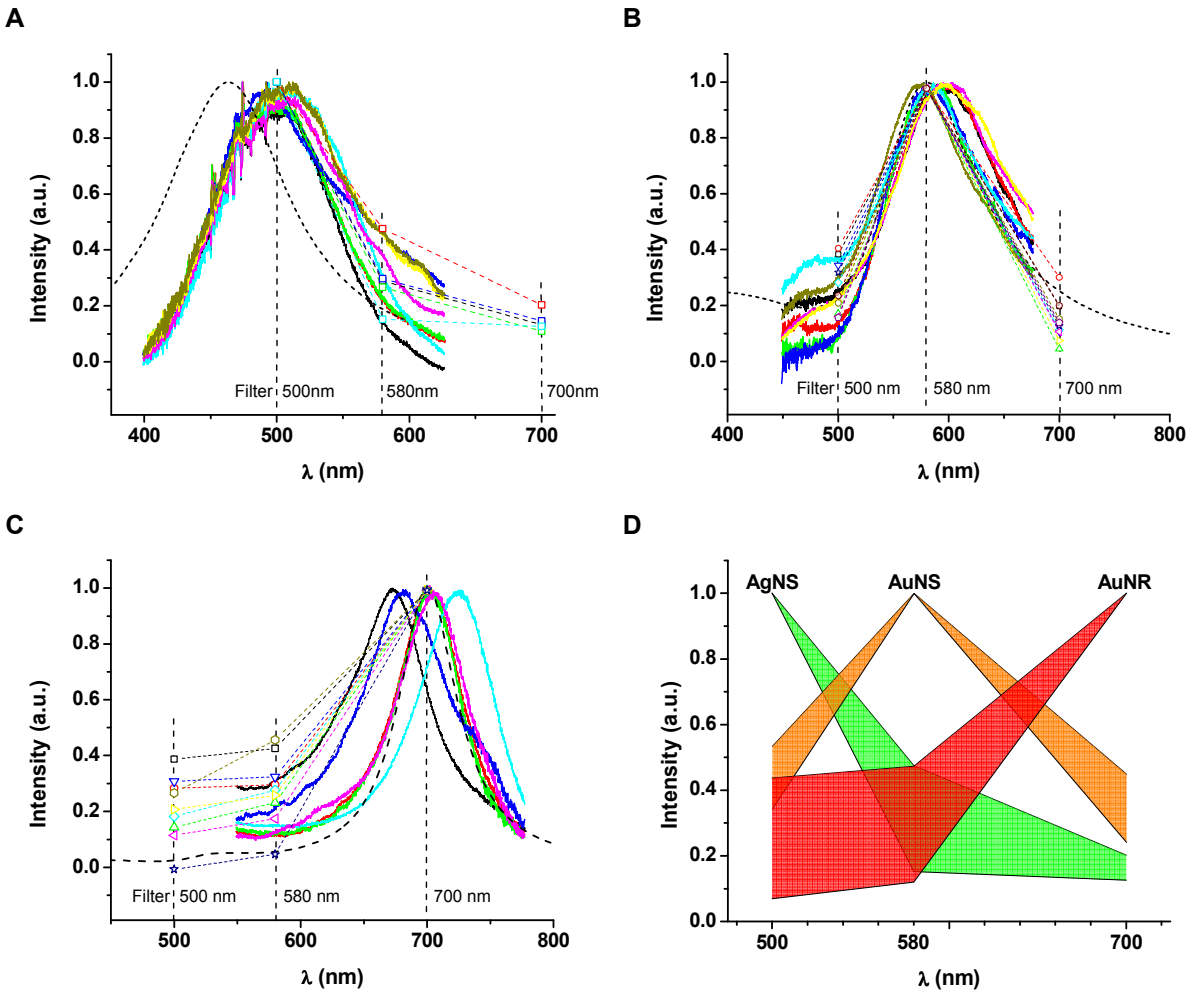

View Article Online
DOI: 10.1039/C6NR01257D

distribution of experimental intensities obtained with the spectral filters. These results were used for the construction of the look-up table (Fig. 4D) that serve as a reference for further automatic 3 points NP spectral discrimination.

The multiplexed immunoplasmonics microscopy was applied for identification of CD44, EGFR and $K_V1.1$ biomarkers on $CD44^+$ $EGFR^+$ $K_V1.1^+$ MDA-MB-231 cells. These cells were incubated during 3 h with mixture of CD44-AgNSs, EGFR-AuNSs and $K_V1.1$-AuNRs, washed, fixed and observed with 3D RLM and the spectral filters. Total number of each type of fNPs was obtained using the look-up table for fNP spectral identification (Fig. 4D). The resulting false-colour 2D image taking into account the average plasmon peak wavelength of each fNP is presented in Fig. 5A. The number and the spatial distribution of targeted biomarkers can be estimated for cellular analysis from 3D distribution of fNPs (Fig. 5B).

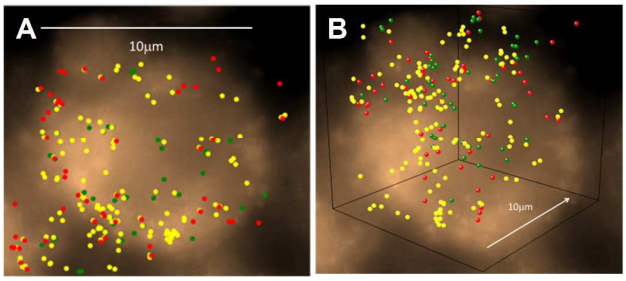

Fig. 5 Identification of CD44, EGFR and $K_V1.1$ cell surface biomarkers on $CD44^+$ $EGFR^+$ $K_V1.1^+$ MDA-MB-231 cells by 3D RLM and 3 points spectral analysis (green: CD44-AgNS, yellow: EGFR-AuNS, red: $K_V1.1$-AuNR (53 nm x 107 nm), objective 100×). 2D (A) and 3D (B) distribution of fNPs. Representative images were obtained from two independent experiments (n = 3).

The next experiments were performed to compare the selectivity and sensitivity of immunofluorescence and immunoplasmonics detection (Fig. 6). The expression levels of targeted cell surface biomarkers on MDA-MB-231 and 661W cells were detected by immunofluorescence imaging (Fig. 6A–F). Human cancer MDA-MB-231 cells expressed strongly CD44 and at a lower level EGFR and $K_V1.1$ (Fig. 6A–C). Low level of $K_V1.1$ was detected on 661W cells in the absence of CD44 or EGFR (Fig. 6D–F). Exposure time was 80 ms for Abs anti-CD44 and 500 ms for Abs anti-EGFR and anti-$K_V1.1$. Background signals from secondary fluorescent Abs were low in the absence of primary Abs (Fig. S8). By increasing the exposure time, fluorescence background and photobleaching can become more important. This problem is solved with immunoplasmonics. The primary Abs used for immunofluorescence were then functionalized on NPs for immunoplasmonics. The $CD44^+$ $EGFR^+$ $K_V1.1^+$ MDA-MB-231 cells and reference $CD44^-$ $EGFR^-$ $K_V1.1^+$ 661W cells were incubated during 3 h with CD44-AgNSs, EGFR-AuNSs and $K_V1.1$-AuNRs, washed, fixed and observed using immunoplasmonics (Fig. 6G–L). A large number of CD44-AgNSs and EGFR-AuNSs were observed on MDA-MB-231 cells, and a smaller number of $K_V1.1$-AuNRs were observed on both MDA-MB-231 and 661W cells. Similar results were obtained by simultaneous addition of the three types of fNPs in 2D (Fig. 7). These results obtained with immunoplasmonics are in a very good agreement with those obtained with immunofluorescence, thus confirming the proposed method's reliability.

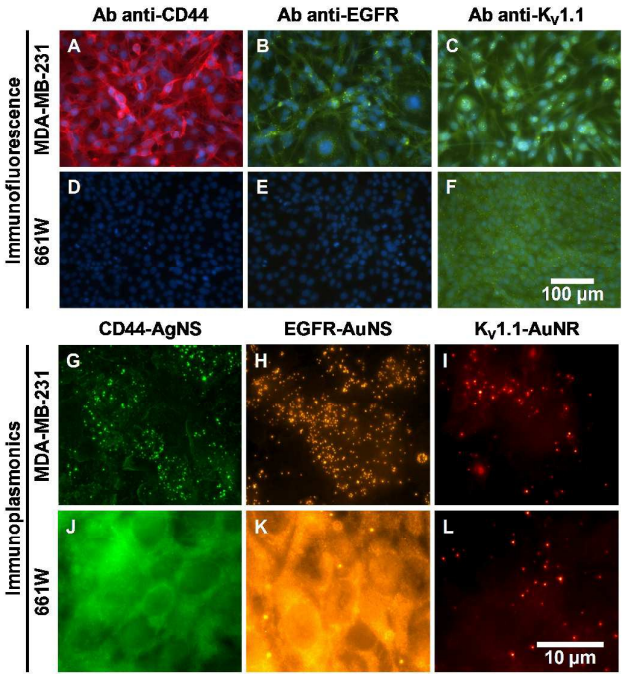

Fig. 6 Identification of CD44, EGFR and $K_V1.1$ cell surface biomarkers on $CD44^+$ $EGFR^+$ $K_V1.1^+$ MDA-MB-231 and $CD44^-$ $EGFR^-$ $K_V1.1^+$ 661W cells by immunofluorescence and immunoplasmonics. (A-F) Immunofluorescence with primary Abs detected with fluorescently-labelled secondary Abs: red-emitting Cy3 conjugated to goat anti-rat IgG Abs (A and D, exposure time of 80 ms) or green-emitting Alexa Fluor 488 dye conjugated to goat anti-mouse (B and E, exposure time of 500 ms) or goat anti-rabbit (C and F, exposure time of 500 ms) IgG Abs (Objective 20× with additional 1.5× magnification). Cell nuclei were stained with 4',6-diamidino-2-phenylindole dihydrochloride (DAPI, blue). Representative images were obtained from four independent experiments. (G-L) RLM with cells incubated for 3 h with 8 µg mL^{-1} CD44-AgNSs, EGFR-AuNSs and $K_V1.1$-AuNRs (40 nm x 92 nm, objective 100×). Representative images were obtained from three independent experiments.

View Article Online
DOI: 10.1039/C6NR01257D

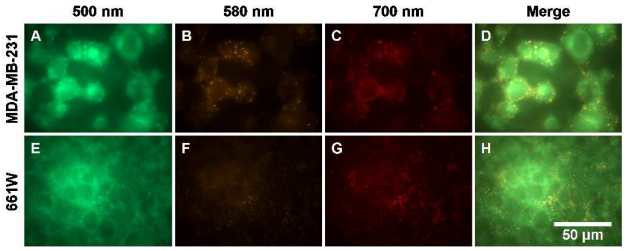

Fig. 7 2D image of CD44-AgNSs, EGFR-AuNSs and $K_V1.1$-AuNRs (53 nm x 107 nm) on $CD44^+$ $EGFR^+$ $K_V1.1^+$ MDA-MB-231 and $CD44^-$ $EGFR^-$ $K_V1.1^+$ 661W cells by using RLM and spectral filters at 500, 580 and 700 nm (green: CD44-AgNS, orange: EGFR-AuNS, red: $K_V1.1$-AuNR, objective 100×). Representative images were obtained from two independent experiments (n = 3).

3. Experimental

3.1. Materials

Rat IgG2a monoclonal Abs anti-human CD44 (Hermes-1, ab119335, 1 mg mL^{-1}) and mouse IgG2b monoclonal Abs anti-human EGFR (EGFR1, ab30, 1 mg mL^{-1}) were purchased from Abcam (Toronto, ON, Canada). Rabbit polyclonal Abs anti-$K_V1.1$ (APC-161, 0.8 mg mL^{-1}) were purchased from Alomone Labs (Jerusalem, Israel). OPSS-PEG(5 kDa)-NHS and HS-PEG (5kDa) were purchased from Nanocs (New York, NY, U.S.A.). AgNSs were purchased from Ted Pella (Redding, CA, U.S.A.), AuNSs and AuNRs were purchased from Nanopartz (Loveland, CO, U.S.A.) (Table S1). Citrate-capped AgNSs, AuNSs and AuNRs were stored at 4 °C in the dark to minimize photoinduced oxidation. Methanol was purchased from VWR International (Mississauga, ON, Canada). NaCl, Na_2CO_3, phosphate-buffered saline (PBS) and 4',6-diamidino-2-phenylindole dihydrochloride (DAPI) were obtained from Sigma-Aldrich (Oakville, ON, Canada). Dulbecco's Modified Eagle's Medium (DMEM containing 4.5 g L^{-1} D-glucose, 584 mg L^{-1} L-glutamine and 110 mg L^{-1} sodium pyruvate), penicillin 10,000 units mL^{-1}, streptomycin 10,000 µg mL^{-1}, trypsin 0.25%-EDTA, fetal bovine serum (FBS), secondary fluorescently-labelled Abs (Alexa Fluor 488 dye conjugated to goat anti-mouse or goat anti-rabbit IgG (H+L) and Cy3 dye conjugated to goat anti-rat IgG (H+L)) were purchased from Life Technologies (Burlington, ON, Canada). Normal goat serum was purchased from Jackson ImmunoResearch Laboratories (West Grove, PA, U.S.A.). Vectashield mounting medium for fluorescence was purchased from Vector Laboratories (Burlingame, CA, U.S.A.). Water was purified with a Millipore treatment system (18.2 MΩcm, Etobicoke, ON, Canada).

3.2. Antibody conjugation to OPSS-PEG-NHS

The NHS end function of OPSS-PEG-NHS was coupled to Ab's amine residues through an amide linkage to provide great conformational freedom and improve its efficiency for binding with the targeted biomarker. The Abs stored in PBS were diluted at 0.1 mg mL^{-1} in aqueous Na_2CO_3 10 mM pH 8.5. Then 9 parts of these Abs were quickly added to a filtered solution of OPSS-PEG-NHS diluted in Na_2CO_3 10 mM pH 8.5 (58.9 µg mL^{-1}). The reaction mixtures (100 µg mL^{-1}, Ab:OPSS-PEG-NHS molar ratio: 1:1.88) were vortexed briefly and kept at 4 °C for 3 h. Aliquots of the solutions were kept at -20 °C until use.

3.3. Functionalization of NPs

NPs were prepared by following a procedure reported previously[17,20,23] with modifications. An aqueous solution of citrate-capped NPs (2 mL) was treated with aqueous Na_2CO_3 10 mM pH 8.5 (222 or 212 µL) and a solution of OPSS-PEG-Ab (0 or 10 µL, 100 µg mL^{-1}) to reach a volume of 2.222 mL. The OPSS end's disulfide group of OPSS-PEG-Ab complex form strong covalent bonds with the NP surface made of Ag or Au.[14,17] The remaining free sites on the NPs were blocked with thiolated PEG chains which can assemble into a densely packed coating. After 1 h incubation at 4 °C, an aqueous solution of HS-PEG (247 µL, 0.4 mM) preventing NPs aggregation in saline environment was added to the suspensions of NPs-PEG-Ab. Water or HS-PEG was also added to suspensions of NPs prepared under the same conditions (2 mL NPs treated with 222 µL Na_2CO_3 10 mM pH 8.5). After 1 h incubation at 4 °C, two samples (320 µL) were taken for analysis. A sample (1.65 mL) was subjected to centrifugation at 4610 g during 2 min. The supernatant was then removed and replaced with 1.34 mL phenol red-free DMEM. Aliquots of the resulting mixtures (320 µL) were treated with water or 10% NaCl (35.5 µL) at 4 °C during 30 min and analysed by UV-visible-NIR spectroscopy in a 96-well plate.

3.4. UV-visible-NIR spectroscopy measurements

UV-visible-NIR absorption spectra (300 to 900 nm, 2 nm step) were acquired with an Epoch microplate spectrophotometer (BioTek Instruments, Winooski, VT, U.S.A.) controlled with the Gen5 Data Analysis software version 1.11.5. A blank spectrum (solvent without NPs) was subtracted from each sample spectrum.

3.5. Cell culture

Human MDA-MB-231 breast cancer and mouse 661W photoreceptor cell lines (American Type Culture Collection, Manassas, VA, U.S.A.) were cultured at 5000 cells/cm^2 in cell culture-treated polystyrene T75 flasks (Sarstedt, Saint-Léonard, QC, Canada). Cells were grown in DMEM supplemented with 10% FBS and antibiotics (100 units mL^{-1} penicillin and 100 µg mL^{-1} streptomycin, 1% PS) in a humidified incubator at 37 °C under a 5% CO_2 atmosphere. Confluent cells were removed by trypsinization and seeded for experiments in DMEM supplemented with 10% FBS/1% PS.

3.6. Immunofluorescence microscopy

Cells were grown in 8-well glass chamber slides (75,000 cells/well, BD Biosciences, Mississauga, ON, Canada). After 2 days, the cells were washed once with PBS, then fixed with ice-cold 70% methanol/30% acetone for 5 min. The samples were blocked with 10% normal goat serum diluted in PBS for 1 h at 20 °C. All subsequent steps were followed by three PBS washes. The cells were incubated for 1.5 h with 1% (v/v)

View Article Online
DOI: 10.1039/C6NR01257D

primary Abs. Then, 1% (v/v) secondary fluorescently-labelled Abs were incubated with the cells for 1.5 h. The cell nuclei were stained with 2.5 μg mL^{-1} DAPI for 5 min and the slides mounted with Vectashield. Samples were examined with an Eclipse Ti microscope (Nikon, Mississauga, ON, Canada) equipped with a 20× objective (NA = 0.45, Nikon), a 60× objective (NA = 0.7, Nikon), a 100× oil immersion objective (variable numerical aperture NA = 0.5–1.3), an available additional 1.5× magnification, a darkfield condenser (NA = 0.95–0.80, Nikon), three commonly used filters (ET-DAPI (ex 350±25, em 460±25), ET-GFP (ex 470±20, em 525±25), ET-DsRED (ex 545±15, em 620±30), Chroma Technology, Bellows Falls, VT, U.S.A.), a fluorescence lamp C-HGFI Intensilight (Nikon) and a QIClick monochromatic digital CCD camera (QImaging, Surrey, BC, Canada). Pictures were taken with the NIS-Elements BR microscope imaging software version 4.00.03 (Nikon).

3.7. Immunoplasmonics microscopy

Cells were seeded onto 19.625 cm^2 glass bottom dishes (5000 cells/cm^2, MatTek, Ashland, MA, U.S.A.). At 85% confluence, cells were washed once with PBS before adding NPs diluted to 8 μg mL^{-1} in DMEM/10% FBS/1% PS.[20] After 3 h incubation at 37 °C, cells were washed three times with PBS to remove unbound NPs and fixed with ice-cold methanol during 10 min at 20 °C. Samples were examined with immunoplasmonics microscopy. The RLM system for 3D wide-field and spectral imaging of NPs-cells was built on the basis of the inverted Eclipse Ti microscope used for immunofluorescence imaging. A flat top inverted microscope motorized stage (ProScan, Prior Scientific, Rockland, MA, U.S.A.) equipped with a z-translation motor allowed fine 3D spatial sample translation and fast z-scanning. A standard white light source (Nikon) with 50 W halogen lamp provided smooth illumination spectrum in the operating range from 450 to 700 nm. Optical beamsplitter (90:10) and spectral 10 nm bandpass filters (Thorlabs, Newton, NJ, U.S.A.) at 500, 580 and 700 nm were used to produce illumination with limited spectral range to ensure spectral discrimination and 3D imaging of detected fNPs. 3D deconvolution (ImageJ, National Institutes of Health, U.S.A.) was applied using experimental PSFs.

For single NP microspectroscopy, the microscope image of a single plasmonic NP, which appears as an isolated bright dot, was aligned with the input slit on an imaging spectrograph (Shamrock 550, Andor Technology, Belfast, UK) equipped with a CCD detecting camera (Newton 940, 2048 x 512 pixels, Andor Technology) and a 150 lines/mm grating providing 364 nm bandwidth. The corrected spectrum intensity was obtained by using the background spectrum adjacent to the single NP and the spectrum of the white light standard reference (Edmund Optics, Barrington, NJ, U.S.A.).[37] A custom-written LabView software (National Instruments, Austin, TX, U.S.A.) controlled the motorized stage displacements and performed 3D image acquisition.

3.8. Statistical analysis

Results are expressed as means ± standard deviation (SD) in all experiments. Statistical computations were performed with GraphPad Instat 3.00 software (GraphPad Software, San Diego, CA, U.S.A.). The Tukey-Kramer multiple comparison test (ANOVA) was used. Values were considered significantly different if $p < 0.05$.

4. Conclusions

Selective labelling of human $CD44^+$ $EGFR^+$ $K_V1.1^+$ MDA-MB-231 cancer cells and reference $CD44^-$ $EGFR^-$ $K_V1.1^+$ 661W cells was achieved with stable CD44-AgNSs, EGFR-AuNSs and K_V1.1-AuNRs in cell culture medium containing serum proteins. The developed immunoplasmonics technology for cell imaging is simple and compatible with standard fluorescence microscopy set-ups. Immunoplasmonics microscopy allows fast counting, identification and 3D localization of fNPs targeting different cell surface biomarkers, and it can offer an extended multiplexing capacity for detecting various biomarkers by taking advantage of the wide distribution of plasmon peaks from different plasmonic fNPs. Experimental demonstration of the immunoplasmonics microscopy with spectral filters corresponding to the plasmonic peak wavelengths of each type of fNP can benefit from recent development in the field of high power LED sources and sensitive imaging camera working from visible to near-infrared (NIR). Final set-up can be designed as independent microscopy system or rather simple upgrade to existing epi-fluorescence microscopes. This technology based on immunoplasmonics microscopy of biomarkers is ready for biological and clinical applications as a cost-efficient alternative to immunofluorescence.

Acknowledgements

This work was supported by the Natural Science and Engineering Research Council of Canada. EB received funding from Fonds de recherche du Québec – Santé. Dr. Laudine Desreumaux-Communal and Prof. Anne-Marie Mes-Masson from CRCHUM are acknowledged for fruitful discussions.

References

1 J. Aaron, N. Nitin, K. Travis, S. Kumar, T. Collier, S. Y. Park, *et al.*, *J. Biomed. Opt.*, 2007, **12**, 034007.
2 M. J. Crow, G. Grant, J. M. Provenzale and A. Wax, *Am. J. Roentgenol.*, 2009, **192**, 1021–1028.
3 V. Biju, T. Itoh, A. Anas, A. Sujith and M. Ishikawa, *Anal. Bioanal. Chem.*, 2008, **391**, 2469–2495.
4 H. S. Choi and J. V. Frangioni, *Mol. Imaging*, 2010, **9**, 291–310.
5 C. Yu, H. Nakshatri and J. Irudayaraj, *Nano Lett.*, 2007, **7**, 2300–2306.
6 F. T. Lee-Montiel, P. Lib and P. I. Imoukhuede, *Nanoscale*, 2015, **7**, 18504–18514.

View Article Online
DOI: 10.1039/C6NR01257D

7 K. D. Wegner and N. Hildebrandt, *Chem. Soc. Rev.*, 2015, **44**, 4792–4834.
8 P. Zhang, S. Lee, H. Yu, N. Fang and S. H. Kang, *Sci. Rep.*, 2015, **5**, 11447.
9 K. Seekell, M. J. Crow, S. Marinakos, J. Ostrander, A. Chilkoti and A. Wax, *J. Biomed. Opt.*, 2011, **16**, 116003.
10 X. Huang, P. K. Jain, I. H. El-Sayed and M. A. El-Sayed, *Nanomedicine*, 2007, **2**, 681–693; A. Taylor, K. M. Wilson, P. Murray, D. G. Fernig and R. Lévy, *Chem. Soc. Rev.*, 2012, **41**, 2707–2717; K. Weintraub, *Nature*, 2013, **495**, S14–S16; J. Yguerabide and E. E. Yguerabide, *J. Cell. Biochem.*, 2001, **84**, 71–81.
11 S. Kumar, J. Aaron and K. Sokolov, *Nat. Protoc.*, 2008, **3**, 314–320.
12 E. E. Connor, J. Mwamuka, A. Gole, C. J. Murphy and M. D. Wyatt, *Small*, 2005, **1**, 325–327; R. Shukla, V. Bansal, M. Chaudhary, A. Basu, R. R. Bhonde and M. Sastry, *Langmuir*, 2005, **21**, 10644–10654.
13 Y.-S. Chen, Y.-C. Hung, I. Liau and G. S. Huang, *Nanoscale Res. Lett.*, 2009, **4**, 858–864.
14 C. Pang, A. Brunelli, C. Zhu, D. Hristozov, Y. Liu, E. Semenzin, *et al.*, *Nanotoxicology*, 2015, **12**, 1–11; J. Yang, Z. Wang, S. Zong, C. Song, R. Zhang and Y. Cui, *Anal. Bioanal. Chem.*, 2012, **402**, 1093–1100.
15 D. J. Javier, N. Nitin, D. M. Roblyer and R. Richards-Kortum, *J. Nanophotonics*, 2008, **2**, 23506.
16 G. A. Craig, P. J. Allen and M. D. Mason, in *Methods in Molecular Biology*, ed. S. R. Grobmyer and B. M. Moudgil, Cancer Nanotechnology, Humana Press, Totowa (NJ, U.S.A.), 2010, ch. 12, vol. 624, pp. 177–193; H. Ju, X. Zhang and J. Wang, in *NanoBiosensing: Principles, Development and Application*, ed. H. Ju, X. Zhang and J. Wang, Springer, New York (NY, U.S.A.), 2011, ch. 1, pp. 1–38.
17 L. R. Hirsch, N. J. Halas and J. L. West, in *Methods in Molecular Biology*, ed. S. J. Rosenthal and D. W. Wright, NanoBiotechnology Protocols, Humana Press, Totowa (NJ, U.S.A.), 2005, ch. 8, vol. 303, pp. 101–111.
18 J. Aaron, K. Travis, N. Harrison and K. Sokolov, *Nano Lett.*, 2009, **9**, 3612–3618; L. L. Ma, J. O. Tam, B. W. Willsey, D. Rigdon, R. Ramesh, K. Sokolov, *et al.*, *Langmuir*, 2011, **27**, 7681–7690.
19 I. H. El-Sayed, X. Huang X and M. A. El-Sayed, *Nano Lett.*, 2005, **5**, 829–834; T. Gong, M. Olivo, U. S. Dinish, D. Goh, K. V. Kong and K.-T. Yong, *J. Biomed. Nanotechnol.*, 2013, **9**, 985–991.
20 E. Bergeron, C. Boutopoulos, R. Martel, A. Torres, C. Rodriguez, J. Niskanen, *et al.*, *Nanoscale*, 2015, **7**, 17836–17847.
21 E. Lee, Y. Hong, J. Choi, S. Haam, J.-S. Suh, Y.-M. Huh, *et al.*, *Nanotechnology*, 2012, **23**, 465101.
22 S. Patskovsky, E. Bergeron and M. Meunier, *J. Biophotonics*, 2015, **8**, 162–167.
23 S. Patskovsky, E. Bergeron, D. Rioux and M. Meunier, *J. Biophotonics*, 2015, **8**, 401–407.
24 K. Subik, J.-F. Lee, L. Baxter, T. Strzepek, D. Costello, P. Crowley, *et al.*, *Breast Cancer: Basic Clin. Res.*, 2010, **4**, 35–41.
25 C. Sheridan, H. Kishimoto, R. K. Fuchs, S. Mehrotra, P. Bhat-Nakshatri, C. H. Turner, *et al.*, *Breast Cancer Res.*, 2006, **8**, R59.
26 G. Maiorano, S. Sabella, B. Sorce, V. Brunetti, M. A. Malvindi, R. Cingolani, *et al.*, *ACS Nano*, 2010, **4**, 7481–7491; A. E. Nel, L. Mädler, D. Velegol, T. Xia, E. M. V. Hoek, P. Somasundaran, *et al.*, *Nat. Mater.*, 2009, **8**, 543–557; A. Salvati, A. S. Pitek, M. P. Monopoli, K. Prapainop, F. B. Bombelli, D. R. Hristov, *et al.*, *Nat. Nanotechnol.*, 2013, **8**, 137–143.
27 U. S. Dinish, G. Balasundaram, Y.-T. Chang and M. Olivo, *Sci. Rep.*, 2014, **4**, 4075; Z. A. Nima, M. Mahmood, Y. Xu, T. Mustafa, F. Watanabe, D. A. Nedosekin, *et al.*, *Sci. Rep.*, 2014, **4**, 4752.
28 S. Schlücker, *ChemPhysChem*, 2009, **10**, 1344–1354.
29 J. C. Y. Kah, M. C. Olivo, C. G. L. Lee and C. J. R. Sheppard, *Mol. Cell. Probes*, 2008, **22**, 14–23; K. Sokolov, M. Follen, J. Aaron, I. Pavlova, A. Malpica, R. Lotan, *et al.*, *Cancer Res.*, 2003, **63**, 1999–2004; N. Nitin, D. J. Javier, D. M. Roblyer and R. Richards-Kortum, *J. Biomed. Opt.*, 2007, **12**, 051505.
30 M. Aioub, B. Kang, M. A. Mackey and M. A. El-Sayed, *J. Phys. Chem. Lett.*, 2014, **5**, 2555–2561; R. Hu, K.-T. Yong, I. Roy, H. Ding, S. He and P. N. Prasad, *J. Phys. Chem. C*, 2009, **113**, 2676–2684.
31 J. D. Unciti-Broceta, V. Cano-Cortés, P. Altea-Manzano, S. Pernagallo, J. J. Díaz-Mochón and R. M. Sánchez-Martín, *Sci. Rep.*, 2015, **5**, 10091.
32 S.-L. Liu, J. Li, Z.-L. Zhang, Z.-G. Wang, Z.-Q. Tian, G.-P. Wang, *et al.*, *Sci. Rep.*, 2013, **3**, 2462.
33 G. Mie, *Ann. Phys.*, 1908, **330**, 377–445.
34 P. B. Johnson and R. W. Christy, *Phys. Rev. B*, 1972, **6**, 4370–4379.
35 E. D. Palik, *Handbook of Optical Constants of Solids*, Academic Press, San Diego (CA, U.S.A.), 1998, 978 p.
36 K. Park and Y. Lee, *J. Toxicol. Environ. Health A*, 2013, **76**, 1236–1245.
37 J. Olson, S. Dominguez-Medina, A. Hoggard, L.-Y. Wang, W.-S. Chang and S. Link, *Chem. Soc. Rev.*, 2015, **44**, 40–57.